Available online at www.sciencedirect.com
SCIENCE DIRECT®
PERGAMON
International Journal of Heat and Mass Transfer 46 (2003) 4105–4117
International Journal of HEAT and MASS TRANSFER
www.elsevier.com/locate/ijhmt

High heat flux removal using water subcooled flow boiling in a single-side heated circular channel

Ronald D. Boyd *, Marcella Strahan, Penrose Cofie, Ali Ekhlassi, Rashad Martin

Thermal Science Research Center (TSRC) College of Engineering, P.O. Box 4208, Prairie View A & M University, Prairie View, TX 77446-4208, USA

Received 18 June 2002; received in revised form 31 January 2003

Abstract

High heat flux removal from plasma-facing components and electronic heat sinks involves conjugate heat transfer analysis of the applicable substrate and flowing fluid. For the present case of subcooled flow boiling inside a single-side heated circular channel, the dimensional results show the significant radial, circumferential and axial variations in all thermal quantities for the present radial aspect ratio (R_o = outside radius to inside radius) of 3.0. A unified, dimensionless representation of the two-dimensional inside wall heat flux, and the dimensional inside wall heat flux ($q_i(\phi, z)$) and temperature ($T_i(\phi, z)$) data was found and used to collapse the data for all circumferential locations. Finally, 2-D boiling curves are presented and are among the first full set of 2-D boiling data presented for a single-side heated circular configuration.
© 2003 Elsevier Ltd. All rights reserved.

Keywords: Single-side heated circular tube; 3-D Water flow boiling

1. Introduction

Since plasma-facing component (PFC) and electronic heat sink (EHS) design requirements, goals and objectives are evolving, the development of a high heat flux removal (HHFR) experimental conjugate multi-dimensional, flow boiling data base will provide the basis for CFD comparisons, flow boiling correlation modifications, and adaptations which include single-side heating effects for detail PFC and EHS flow channel and substrate design studies. This will lead to cost-effective and robust designs. Many papers have been published reporting either new or modified flow boiling correlations. Generally, there appears to be good confidence in predicting water flow boiling for uniformly heated circular channels with or without twisted tapes. However, all PFCs and EHSs involve single-side heated flow channels and hence depend on at least two-dimensional, and in some cases three-dimensional, conjugate data and analysis for new or modified flow boiling or single-phase correlations with two- and possibly three-dimensional influences.

Although HHFR designs and related innovations and improvements have been proposed for the PFCs in the International Thermonuclear Experimental Reactor (ITER) via the Engineering Design Activity by many investigators [1–13], additional divertor and PFC development and certification are ongoing for several new machines [9,14,15]. One principal machine concept being considered is the fusion ignition research experiment (FIRE). As noted by Ulrickson et al. [14], the primary focus of the FIRE program is an understanding of the plasma dominated by alpha heating. However, they also emphasized that a key issue of the FIRE design is HHFR from the outer divertor or PFC. Nygren [16] and Chappuis et al. [17] summarized prior experiences which may improve PFC functionality. Finally, Rödig et al. [18] compared existing electron beam test facilities used in testing HHFR components.

Fundamental HHFR research involving single-side heated flow channels is evolving. Boscary et al. [19]

* Corresponding author. Tel.: +1-936-857-4811; fax: +1-936-857-2325.
E-mail address: ronald_boyd@pvamu.edu (R.D. Boyd).

0017-9310/03/$ - see front matter © 2003 Elsevier Ltd. All rights reserved.
doi:10.1016/S0017-9310(03)00102-9

reported success in: (1) developing a dimensional analysis of the critical heat flux (CHF) in terms of five dimensionless groups, and (2) introducing enhancement factors for single-side heating relative to uniform heating. Further, Boscary, Fabre and Schlosser [20] detected CHF via an infrared camera and noted that their data was "reasonably well" predicted by the sublayer dryout model of Celata et al. Inasaka and Nariari [21] estimated the inside wall heat flux for single-side irradiated flow channels with twisted tapes. Celata et al. [22,23] proposed CHF models which apply to both uniformly-heated and single-side heated channels with and without swirl flow. Liu et al. [24]: (1) reported a CHF model based on liquid layer dryout; (2) made comparisons with a large data bank; (3) displayed parametric trends with respect to several parameters; and, (4) alluded to the model being adaptable to single-side heated flow channels with water, nitrogen and freon-113. Further, Celata et al. [25,26]: (1) made flow visualizations of water subcooled flow boiling, and (2) obtained bubble and hot spot dimensions as a function of thermal-hydraulic test conditions.

The optimized design of single-side heated PFCs and EHSs is dependent on using conjugate heat transfer to find the local distribution of inside wall heat flux on the flow channels of the component or heat sink cooling substrate. For the present physical configuration involving a single-side heated cylindrical-like flow channel with internal forced flow, the local inside wall heat flux and other fundamental convective/flow boiling quantities were obtained from selectively chosen local wall temperatures close to the inside boundary of the flow channel. To this end, three-dimensional thermal measurements for a one-side heated cylindrical-like test section were made. The resulting local wall temperature data were reduced using a theoretical analysis developed by Boyd [27] to produce the circumferential and radial distributions. The following fundamental inside channel wall convective and flow boiling thermal quantities were deduced from local channel wall temperature measurements: (1) inside wall heat flux distribution, (2) inside wall temperature distributions, and (3) local heat transfer coefficients.

2. Analysis

The test section was designed and based on a theoretical analysis of the two-dimensional (radial, r, and circumferential, ϕ), wall temperature distribution in a solid circular tube (with inside and outside radii, r_i and r_o) with internal forced convective flow and: (1) subjected to an external heat flux (q_o) over one-half of the outside perimeter, and (2) with the remaining half of the perimeter insulated. This circular tube is referred to as the "theoretical circular cylinder." For a constant inside mean heat transfer coefficient (h_m), the dimensionless two-dimensional wall temperature distribution is

$$T^*(R,\phi) = \frac{T(r,\phi) - T_b}{\left(\frac{q_o r_o}{k}\right)} = \frac{1}{2}\left(\frac{1}{Bi} + \ln R\right) + \sum_{n=1}^{\infty} \frac{2\sin n\left(\phi + \frac{\pi}{2}\right)}{\pi n^2} \frac{R^n}{R_o^n} \times \frac{(1 - Bi_n R^{-2n})}{(1 + Bi_n R_o^{-2})}, \quad (1)$$

where $n = 1, 3, 5, 7, \ldots$; $R = r/r_i$; $R_o = r_o/r_i$; q_o is the externally applied heat flux; k is the wall thermal conductivity; Bi is the Biot number, $(r_i h_m/k)$; $\phi = 0$ at the heated part of the plane of symmetry; and,

$$Bi_n = \frac{Bi - n}{Bi + n}. \quad (2)$$

The corresponding dimensionless inside wall heat flux is

$$\frac{q_i(\phi)}{q_o} R_0^{-1} = \frac{1}{2} + \sum_{n=1}^{\infty} \frac{4\sin n\left(\phi + \frac{\pi}{2}\right)}{\pi n R_o^n} \times \frac{Bi}{[(Bi + n) + (Bi - n)R_o^{-2n}]}. \quad (3)$$

The nominal cross-sectional dimensions for the experimental test section were based on a value of R_o of 3.0. The actual value for the inside diameter of the test section was selected to be 10.0 mm, which corresponds to typical values used for flow channels in fusion reactor divertors. The resulting values of r_i and r_o make it physically practical to have a test section thick enough to make local wall temperature measurements. One result of the analysis is that multi-dimensional wall effects will be negligible for: (1) $Bi \leqslant 0.01$ when $R_o \geqslant 1.34$, and (2) $Bi \leqslant 0.001$ when $R_o = 1.04$. For these two extrema, the resulting inside channel wall heat flux will not vary in the circumferential direction. For the present experiment, the Bi is anticipated to be of the order of 0.2, which will result in significant circumferential variations of the inside channel wall heat flux. Therefore, the above equations for $T(r,\phi)$ and $q_i(\phi)$ were applied at a given axial location using the local bulk fluid temperature ($T_b(z)$) to reduce the measurements of local wall temperature.

The locally measured wall temperature was used in Eq. (1) to produce a value of Bi, which is hence forth referred to as Bi_c and is then used in Eq. (1) for $R = 1$ and Eq. (3) to obtain corresponding values of the tube inside wall temperature (T_i) and heat flux (q_i), respectively. The subscript "c" is used here to denote this quantity, Bi_c, not as a characterizing Biot number but as a correlation parameter which facilitates extrapolating the measurement over the small distance to the inside boundary. The results will be circumferential distributions at a given axial location; i.e. $T_i(\phi,z)$ and $q_i(\phi,z)$.

Because it was not practical to fabricate a semi-circular shell resistive heater to facilitate the single-side

heating, five flat faces were machined on to the external surface of the "theoretical circular cylinder" to form the cross-section of the actual test section (See Figs. 1 and 2). This configuration was heated with five flat resistive graphite heaters. Although a larger number of heaters would have provided a better approximation, the practical complications of heater installation and stability would have increased. To compensate for this limitation, the test section thickness was chosen to be large, with $R_o = 3.0$.

Calorimetric measurements were used to measure the actual power transferred to the flowing water. The actual power transferred to the water is given in terms of inlet and outlet specific enthalpies by

$$P_a = \dot{m}(h_{outlet} - h_{inlet}), \tag{4}$$

where $\dot{m}$ is the mass flow rate. The actual external, net heat flux is given by

$$q_o = \frac{P_a}{5A_H}, \tag{5}$$

where A_H is the surface area (180.0×9.04 mm^2; i.e., $L_H \times w$) of one of the heaters, L_H is the heater length and w is the heater width.

The local axial bulk fluid temperature was determined from the thermodynamics tables as the temperature corresponding to the following value of the local axial bulk fluid specific enthalpy; i.e.,

$$h_b(z) = h_{inlet} + \frac{5.0 q_o z w}{\dot{m}}. \tag{6}$$

In an effort to collapse the measured data on to a single curve, additional definitions of the dimensionless temperature and inside wall heat flux were obtained from Eqs. (1) and (3) as follows:

$$\theta_T = \frac{T^* - \frac{1}{2}\left(\frac{1}{Bi_c} + \ln R\right)}{\frac{2}{\pi}\frac{R}{R_o}\frac{(1 - Bi_{nc}|_{n=1}R^{-2})}{(1 + Bi_{nc}|_{n=1}R_o^{-2})}}, \tag{7}$$

$$\theta_q = \frac{\frac{q_i}{q_o} - \frac{R_o}{2}}{\frac{4}{\pi}\frac{Bi_c}{[(Bi_c + 1) + (Bi_c - 1)R_o^{-2}]}}, \quad \text{and} \quad Bi_{nc} = \frac{Bi_c - n}{Bi_c + n}. \tag{8}$$

Inspection of the reduced data trends indicates that for a given value of Reynolds number, Bi_c is related to q_o

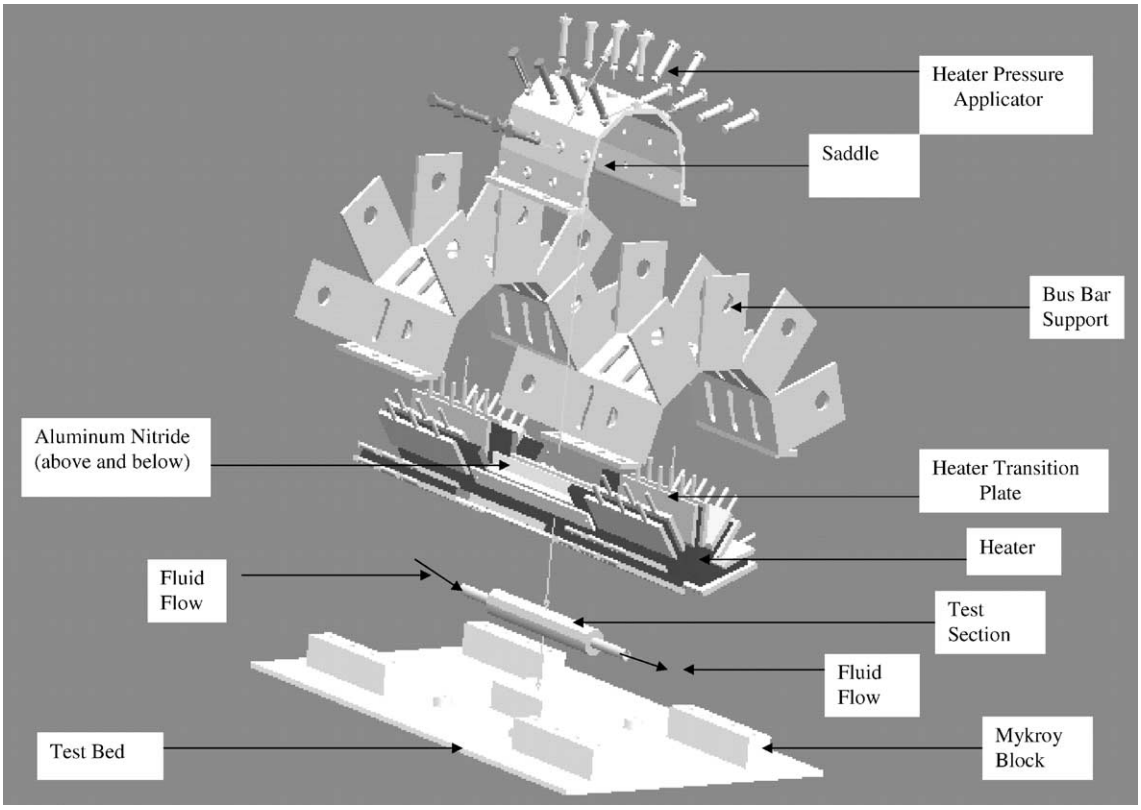

Fig. 1. Test section and expanded test assembly used for HHFR with subcooled flow boiling in a single-side heated flow circular channel.

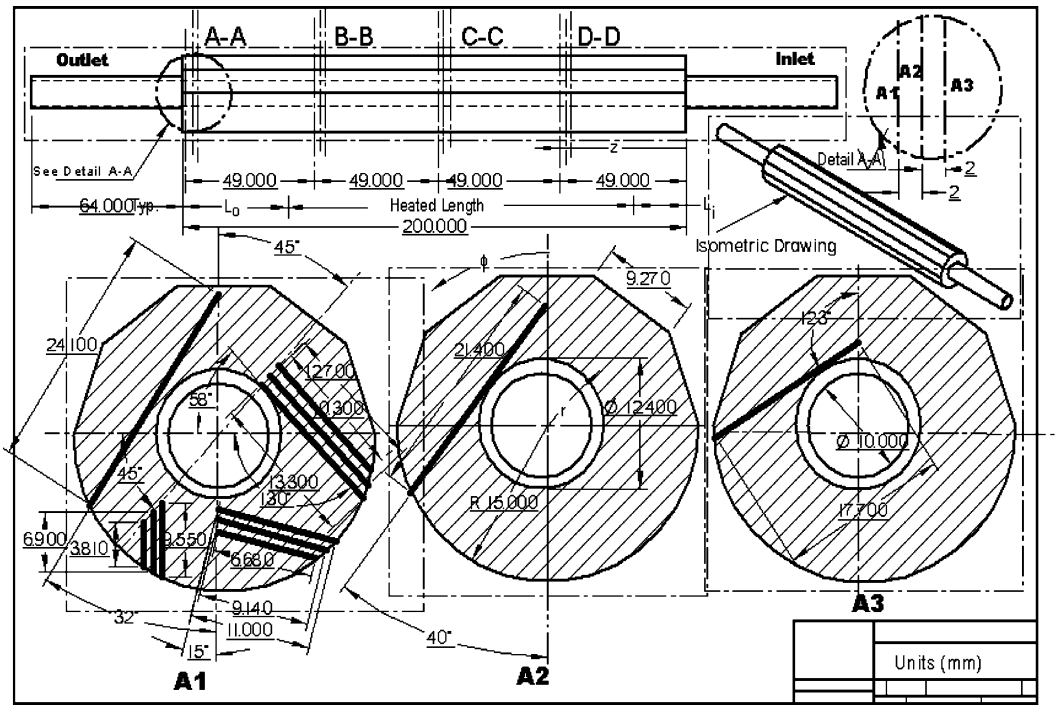

Fig. 2. Test section used for local temperature and heat transfer measurements. Water flows through the 10.0 mm diameter channel. The thermocouple (TC) wells are the solid black lines with specified lengths and angles. The outer concentric circle around the 10.0 mm inner diameter channel should not appear in the shown sections but has been added to show the outside diameter of the channel near the inlet and exit. Note: At $\phi = 0°$, the single TC shown in plane A3 should be switched with the corresponding TC in plane A1.

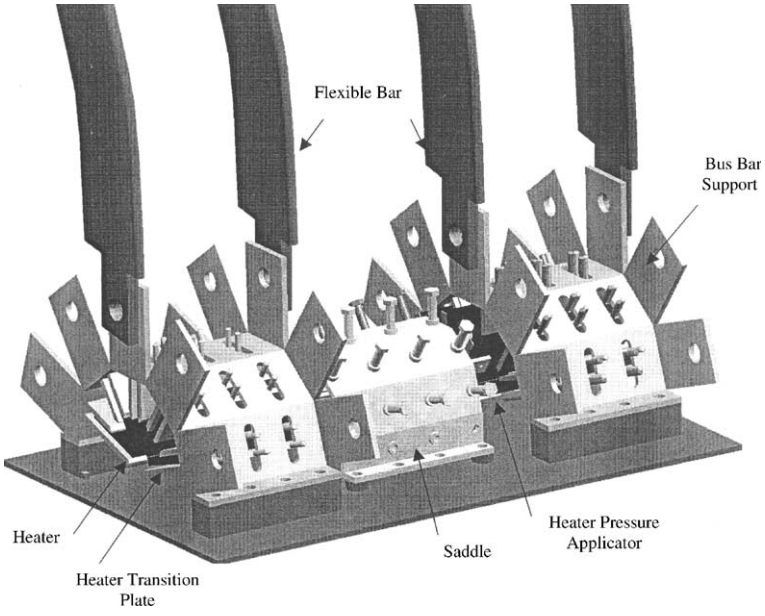

Fig. 3. Test section assembly with heaters and flexible power bus bars used for HHFR with water subcooled flow boiling in a single-side heated circular flow channel.

$(r_o - r_i)/k$, ϕ, and z. Eqs. (7) and (8) were used to expressed the measured data in a further dimensionless form for the temperature (θ_T) and the inside wall heat flux (θ_q). The resulting data was compared and was

collapsed using local values of $T_b(z)$ with the theoretical reduced forms of Eqs. (1) and (2); i.e.,

$$\theta_T = \sin\left(\phi + \frac{\pi}{2}\right) + \sum_{n=3}^{\infty} \frac{\sin n\left(\phi + \frac{\pi}{2}\right) R^{n-1}}{n^2 R_o^{n-1}} \times \frac{(1 - Bi_n R^{-2n})}{(1 + Bi_n R_o^{-2n})} \frac{(1 + Bi_n|_{n=1} R_o^{-2})}{(1 - Bi_n|_{n=1} R^{-2})}, \quad (9)$$

$$\theta_q = \sin\left(\phi + \frac{\pi}{2}\right) + \sum_{n=3}^{\infty} \frac{\sin n\left(\phi + \frac{\pi}{2}\right)}{n R_o^{n-1}} \times \frac{(Bi + 1) + (Bi - 1) R_o^{-2}}{(Bi + n) + (Bi - n) R_o^{-2n}}, \quad (10)$$

where $n = 3, 5, 7, \ldots$

3. Test conditions

The configuration under study (see Fig. 1) consists of a non-uniformly heated cylindrical-like test section with a circular coolant channel bored through the center. The theoretical or idealization of the cylindrical-like test section would be a circular cylinder with half (−90° to +90°) of its outside boundary subjected to a uniform heat flux and the remaining half insulated. The outside diameter of the cylindrical-like test section was 30.0 mm and its length was 200.0 mm. The actual directly heated length (L_H) was 180.0 mm. The inside diameter of the flow channel was 10.0 mm. Water was the coolant. The inlet water temperature can be set at any level in the range from 23.0 to 130.0 °C and the exit pressure can be set at any level in the range from 0.05 to 4.0 MPa. Thermocouples were placed at forty-eight locations inside the solid cylindrical-like test section. For each of four axial stations, three thermocouples were embedded at four circumferential locations (0°, 45°, 165°, and 180°, where 0° correspond to that portion of the plane of symmetry close to the heated surface) in the wall of the test section. Finally, the mass velocity can be set at any level in the range from 0.3 to 10.0 Mg/m^2 s.

The mass velocity and exit pressure used for the present case were 0.59 Mg/m^2 s, and 0.207 MPa (T_{sat} = 121.3 °C), respectively. Typed-J thermocouples with a 0.5 mm diameter were used and calibrated to within ±0.1 °C with a precision calibrator. Other uncertainties include ±0.06 Mg/m^{2}s and ±0.004 MPa for the mass velocity and pressure, respectively. For these test conditions, the basic fluid flow is turbulent ($Re = 6900$) and

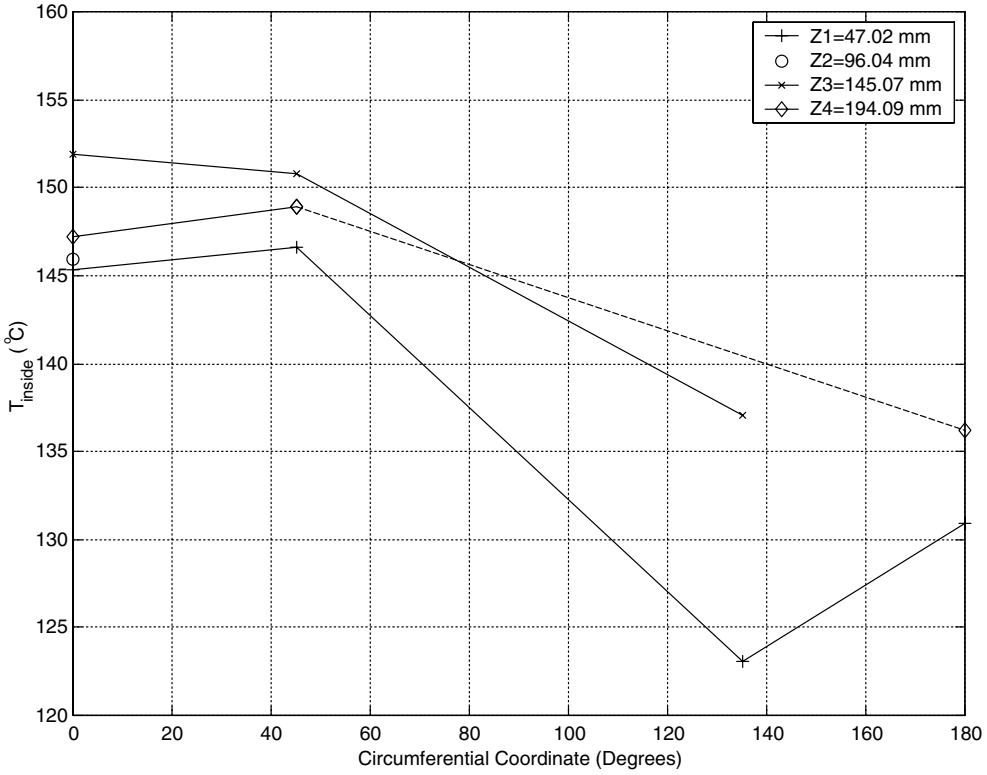

Fig. 4. Circumferential variations of the inside circular-like test section water flow channel wall temperature (T_i) at different axial locations and derived from measurements made at radial locations about midway between the heated and cooled boundaries for an outside (or incident) single-side heat flux of 728.3 kW/m^2.

highly developing with a reciprocal Graetz number (Gz^{-1}) of 4.5×10^{-4}. A detail description of the test facility, experimental, and measurement details are given elsewhere by Boyd et al. [28].

The test section was subjected to successively higher heat fluxes over a period of time; and at each level of heat flux, a quasi-steady state was allowed to occur before the heat flux was increased again. As a result, the experimental data (which includes local temperature, pressure, flow rate, voltage, current, etc.) were recorded as a function of time during the entire course of the experiment; and, several quasi-steady states [29] occurred and included flow regimes ranging from single-phase flow up to fully-developed subcooled flow boiling. Consequently, a three-dimensional distribution of the local test section wall temperature was measured for each quasi-steady state from single-phase flow to fully-developed subcooled flow boiling.

4. Test section

The test sections (see Fig. 2) were fabricated from Type AL-15 Glidcop Grade Copper. The overall length of the test section, including the inlet and outlet reduced diameter sections, is 328.0 mm. The main section of the test section (available for heating) is 200.0 mm long with a nominal outside diameter of 30.0 mm and an inside diameter of 10.0 mm. For these tests, the actual heated length, L_H, was 180.0 mm. In Fig. 2, both isometric and longitudinal side views are shown. The flow channel inlet and exit are indicated in the latter view. Also shown in the latter view are four axial stations labeled A–A, B–B, C–C, and D–D, which are axial locations where 1.19 mm diameter thermocouple (TC) wells exist for local in-depth wall temperature measurements. The purpose of the four axial locations is to obtain an estimate of the axial distribution of the test section wall temperature for a given applied heat flux. Since the geometry of the TC wells is identical at all four primary axial stations, a detail description will be given for only one axial station. For example, the A–A axial station in Fig. 2 has twelve (12) TC wells. Ten (10) of the TC wells are in plane A1; and, one TC well is in plane A2 and another TC well is in plane A3. Planes A2 and A3 are axially displaced upstream from plane A1 by 2.0 and 4.0 mm, respectively. Graphite powder was used in the cavity between the TC and the wall of the TC well to establish a good

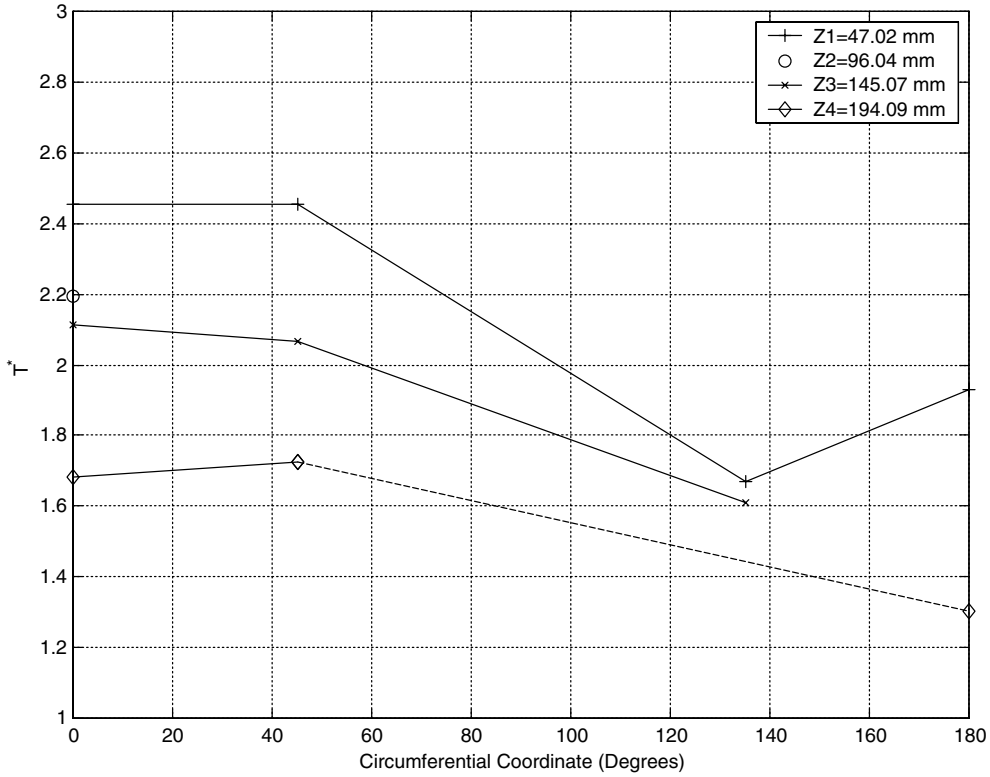

Fig. 5. Circumferential variations of the inside circular-like test section water flow channel dimensionless wall temperature (at $R = 1$) at different axial locations and derived from measurements made at radial locations about midway between the heated and cooled boundaries for an outside (or incident) single-side heat flux of 728.3 kW/m^2.

thermal bond. Finally, the lengths L_i and L_o shown in Fig. 2 are variable lengths whose sum must equal 20.0 mm for a given experimental setup.

The TCs at station A–A will give both radial and circumferential distributions of the local wall temperature. Hence, a combination of all axial stations will produce a three-dimensional distribution of the test section local wall temperature as a function of the applied heat flux and the water flow regime which may vary from single-phase at the test section inlet to subcooled flow boiling at the exit.

The single-side applied heat flux comes from a 350.0 kW DC power supply which provides resistive heating to the test section via five (5), grade G-20 graphite flat heaters which are shown in Fig. 1 and each placed over a 1.0 mm thick aluminum nitride layer which in turn rests on each of the five (5) flat sides of the test section. The aluminum nitride is used for two important purposes: (1) to electrically isolate the test section from the heaters, and (2) to assure good thermal connection between the test section and the heaters. The power supply provides power to the heater elements in the experimental set-up through a copper bus duct/cabling (bus bar) system which is connected to the test assembly via the bus bar supports shown in Fig. 1. A post-test inspection of the test section was made to verify the positioning and embedded depths of each of the forty-eight test section TCs. Based on a post-test examination of the test section and measurements, a revised test matrix resulted which included thirty-one (31) test section channel wall TCs.

5. Test section assembly

As shown in Fig. 1, the test section assembly is a unique design and allows flow through the test section, heating from one side, and secure positioning of both the test section and heaters. The saddle is used to: (1) secure the position of the heaters relative to the test section; and (2) increase the contact pressure between the heater, the aluminum nitride, and the outside surface of the test section. The latter function of the saddle is essential in reducing the thermal contact resistance between each of these layers.

The saddle and the test section are electrically isolated from the heater by a 0.5 mm thick layer of aluminum nitride. The complete assembly of all components in Fig. 1 is shown in Fig. 3. The mykroy shown

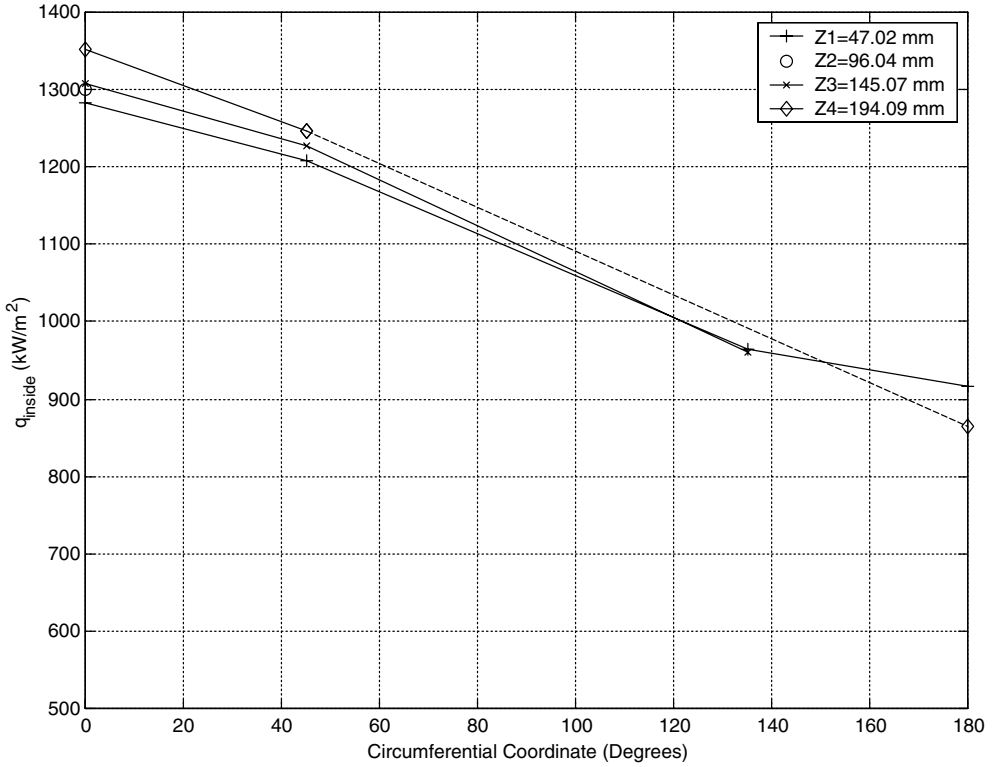

Fig. 6. Circumferential variations of the inside circular-like test section water flow channel wall heat flux (q_i) at different axial locations and derived from measurements made at radial locations about midway between the heated and cooled boundaries for an outside (or incident) single-side heat flux of 728.3 kW/m^2.

serves both as a support for the assembly and as electrical and thermal barriers between the bus bar support and the test bed. Also shown in Fig. 3 are the heater connections to the bus bar support via the heater transition plates. A set of flexible bus bars are used to transfer the electrical current from the rigid copper bus bars to the bus bar support, to the transition plate, and then to the heaters (see Fig. 3).

6. Results

HHFR experiments of a single-side heated circular-like flow channel with internal convection have resulted in two-dimensional distributions of the inside flow channel wall temperature, heat flux and heat transfer coefficient. Results are presented with water as the fluid for flow conditions ranging from single-phase to fully-developed subcooled flow boiling. Water boiling curves and dimensionless representations are presented. A tabulation of the locally-measured (three-dimensional) channel wall temperatures will be made available as a TSRC Data Tabulation. This data contains the effects of conjugate heat transfer with turbulent and subcooled flow boiling. All the data was reduced, used to compute θ_T and plotted along with the right-hand side of Eq. (9). All the data collapsed on to the curve formed from Eq. (9).

6.1. Flow channel inside wall temperature

Fig. 4 shows the circumferential distribution of the inside flow channel wall temperature (T_i) at radial locations about midway between the heated boundary and the fluid-solid (cooling) boundary. The plot is for a net incident outside heat flux of $q_o = 728.3$ kW/m^2. For this outside single-side heat flux, the inside wall heat flux is near 1368.0 kW/m^2 at $z = 194.09$ mm, and $\phi = 0°$. At $\phi = 0°$, T_i increases slightly with z up to the third downstream axial station ($z = 145.07$ mm) and then decreases as the channel exit is approached. As can be seen, the slope of the inside wall temperature profile is near zero at $\phi = 0°$. Since there were at most only four circumferential measurement locations, the circumferential data serve as a guide for the detail distribution. Data interpretation improves when the fact that the slope of the T_i-profile must also be zero at $\phi = 180°$. It should be noted that a dotted line is used in all plots between data

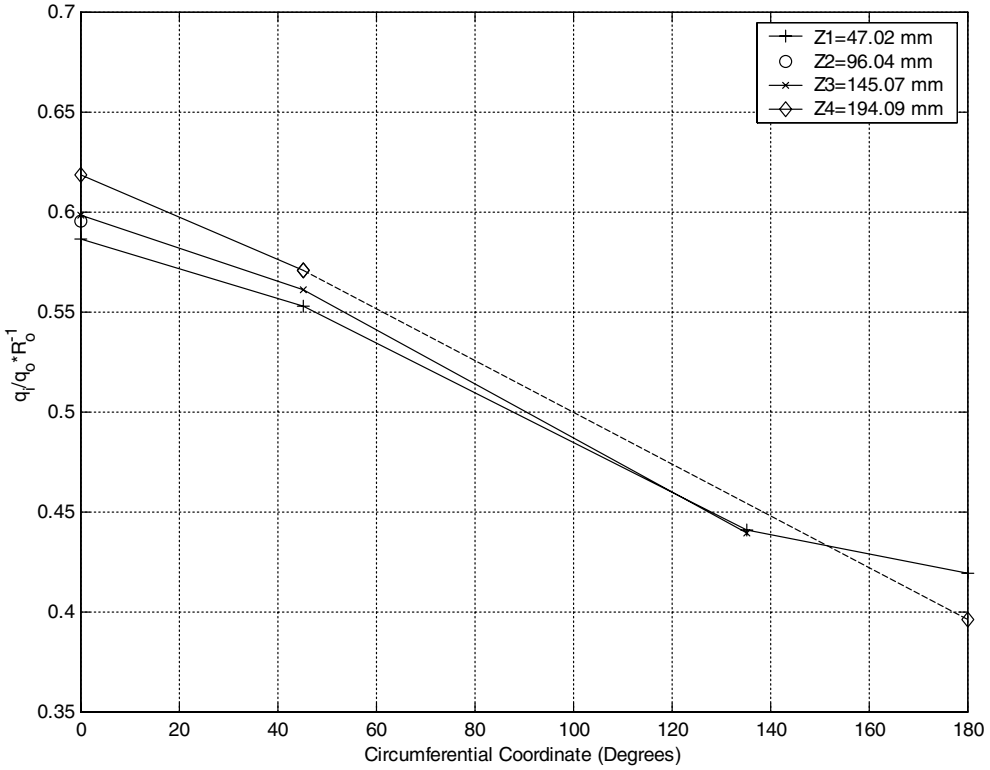

Fig. 7. Circumferential variations of the inside circular-like test section water flow channel dimensionless wall heat flux ($q_i/q_o \times R_o^{-1}$) at different axial locations and derived from measurements made at radial locations about midway between the heated and cooled boundaries for an outside (or incident) single-side heat flux of 728.3 kW/m^2.

points to indicate that there is a missing data point entry between those two points which could have otherwise help to better define the variation between those two points. For example at $z = z_4$ in Fig. 4, a dotted line connecting the right-most data points indicates that a missing data point entry is between those two points. If that entry was not missing, more definition in the circumferential variation would have existed and could have been used possibly to verify the zero-slope condition and better display the variation in T_i as $\phi = 180°$ is approached. This can be illustrated further by the data at $z = z_1$, where all four circumferential data entries are present. While the zero-slope condition at $\phi = 0°$ is apparent, a similar condition at $\phi = 180°$ is only apparent when it is realized that the shown right-most two data points represent bounds for the physical profile as 180° is approached. Data similar to the above inside wall temperature data was generated at twelve additional levels of q_o and are contained in the TSRC Data Tabulation. It should be noted that each point in Fig. 4 is for a slightly different radial location. The exact radial and other coordinate location for each point also is contained in the data tabulation.

The non-dimensional form of T_i is T^* and is presented in Fig. 5. The non-dimensionalization reverses the relative magnitudes of the ordinate (compare Figs. 4 and 5). The representation puts the data points in a form that would be conducive for comparisons with other conjugate heat transfer/flow boiling predictive tools.

6.2. Flow channel inside wall heat flux

The data representing the circumferential, inside wall heat flux (q_i) profile is shown in Fig. 6 for the above noted conditions. The variations with respect to ϕ are substantial and can be seen to be amenable to the zero slope conditions at $\phi = 0$ and 180°. At $\phi = 0°$, q_i increases with z. All thirty-one thermocouple well data were reduced to produce values of q_i. For a given value of ϕ and z, the thermocouple wells closest to the heated boundary resulted in higher values of q_i than the other two locations close to the fluid. It is believed that those wells closest to the fluid boundary will result in better estimates of q_i. Reduced data for q_i at thirteen levels of q_o are contained in the TSRC Data Tabulation from each of the thirty-one measurements. The reduced data for q_i and T_i and the data for $T(r, \phi, z)$ form an evolving conjugate heat transfer data-base with influences of turbulence, developing flow, single-side heating, single-phase flow, and flow boiling. The corresponding values of the local (axial) bulk fluid (water) temperature are contained also in the TSRC Data Tabulation. The representation of the inside heat flux in dimensionless form is given in Fig. 7.

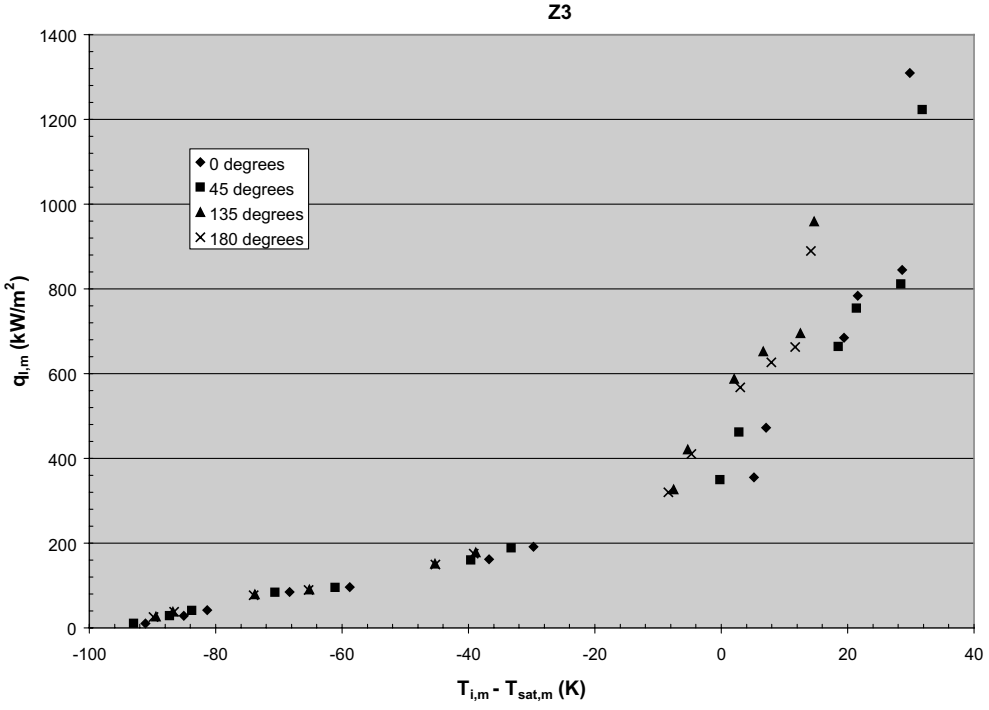

Fig. 8. Local (2-D) water boiling curves at $z = z3 = 143.07$ mm as a function of the circumferential coordinate with $\phi = 0°$ and 180° corresponding to the heated and cooled portions, respectively, of the plane of symmetry of the test section.

7. Local water boiling curves

Two-dimensional (circumferential and axial), local boiling curves are presented for subcooled water flow boiling in a single-side heated circular flow channel. Although a complete compilation of all the reduced data is contained in the above noted tabulations, examples of the 2-D boiling curves are shown in Figs. 8–11. In these figures, $T_{i,m}$ is the mean value of T_i at given values of ϕ and z. In this context, this mean value was obtained from the corresponding three values of T_i resulting from the three radial measurements made at given values of ϕ and z. The water boiling curves in Fig. 8 are for a nominal axial coordinate of $z = z_3 = 143.07$ mm.

The quantitative differences in the circumferential (ϕ) variations of the boiling curve are shown in Fig. 8 for ϕ varying from 0° to 180°. The highest two heat fluxes (right-most pair of similar points) at 0° indicate a fully developed boiling regime exists; and as ϕ increases, the slope of the boiling curve at similar points decreases which indicates that a region of less and less partially developed flow exists. Although these trends exist at all axial locations, the circumferential variations did change for different values of z.

The axial variations are contained in Figs. 8–11. As one would expect, the wall superheat (i.e., $T_i - T_{sat}$) and the above noted slopes at all circumferential locations decrease with z. As z decreases from $z_3 = 143.07$ mm (Fig. 8) to a nominal axial location of $z = z_2 = 94.04$ mm (Fig. 9), there is a change in the polarity of the relative superheat for $\phi = 0°$ and 45° at the highest heat fluxes. As z decreases further to 45.0 mm (Fig. 10), the polarity remains unchanged and the absolute value of the differences in relative superheat increases. However if z increases from z_3 to $z = z_4 = 192.09$ mm (Fig. 11), the polarity does not change; but, the differences in the absolute value of the relative superheat increase. The above noted differences may be due to a redistribution of the flow and/or heat transfer. At values of q_i above those shown in Figs. 8–11, a loud hammer-like sound occurred and increased in amplitude as the heat flux was increased.

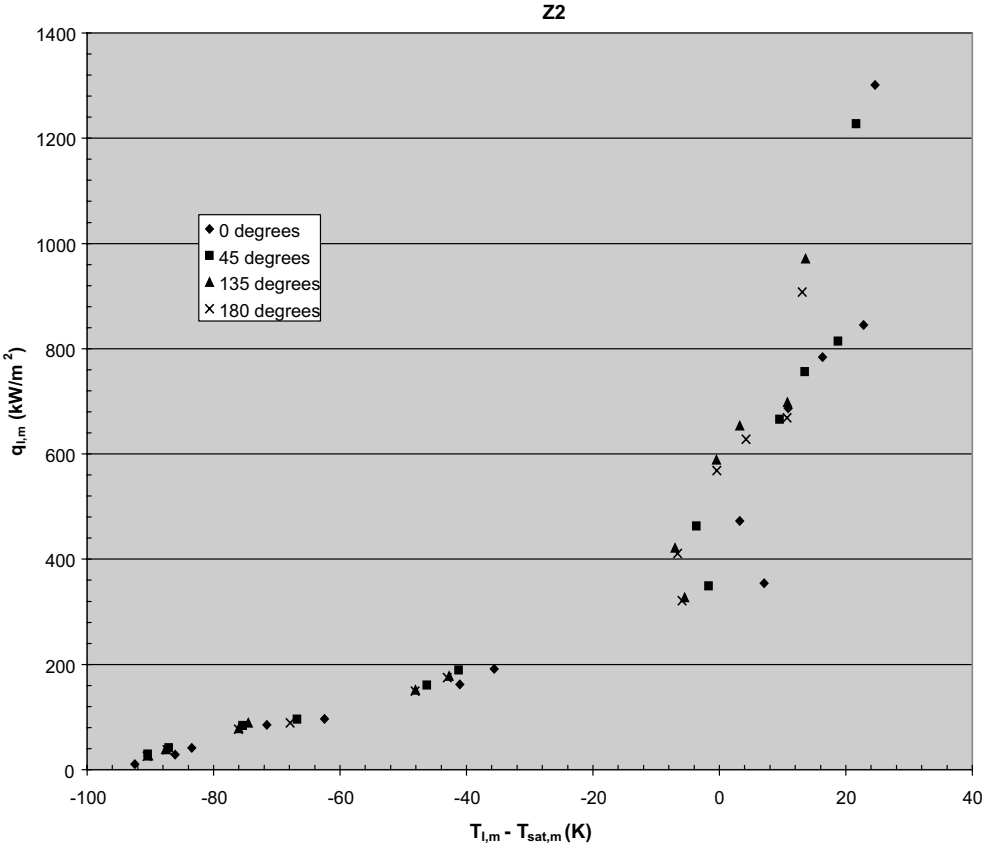

Fig. 9. Local (2-D) water boiling curves at $z = z2 = 94.04$ mm as a function of the circumferential coordinate with $\phi = 0°$ and 180° corresponding to the heated and cooled portions, respectively, of the plane of symmetry of the test section.

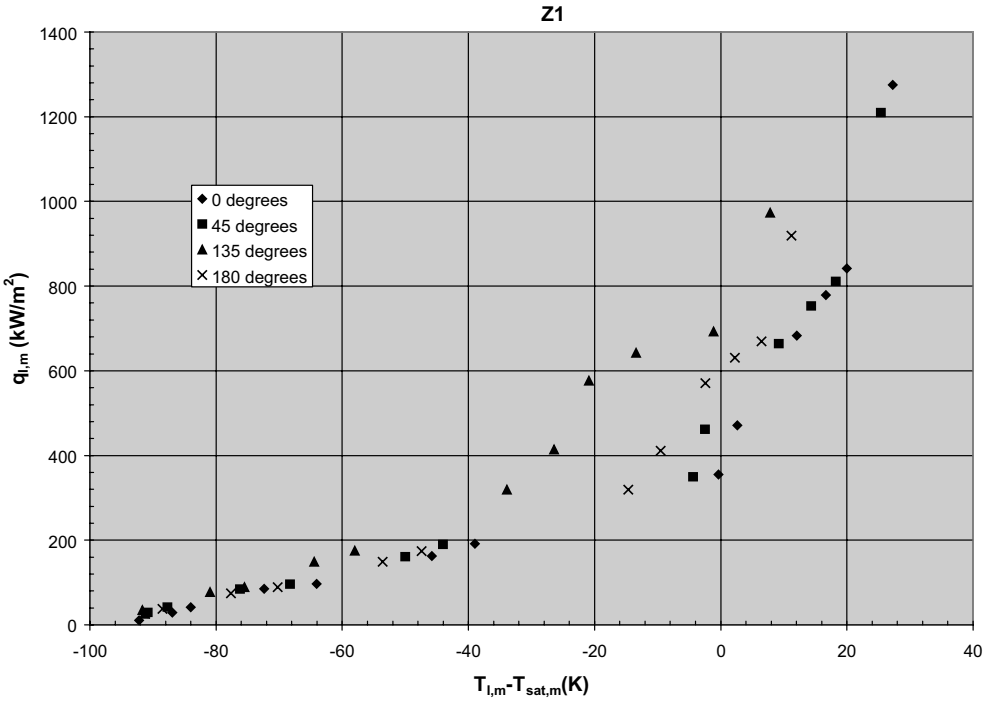

Fig. 10. Local (2-D) water boiling curves at $z = z1 = 45.02$ mm as a function of the circumferential coordinate with $\phi = 0°$ and 180° corresponding to the heated and cooled portions, respectively, of the plane of symmetry of the test section.

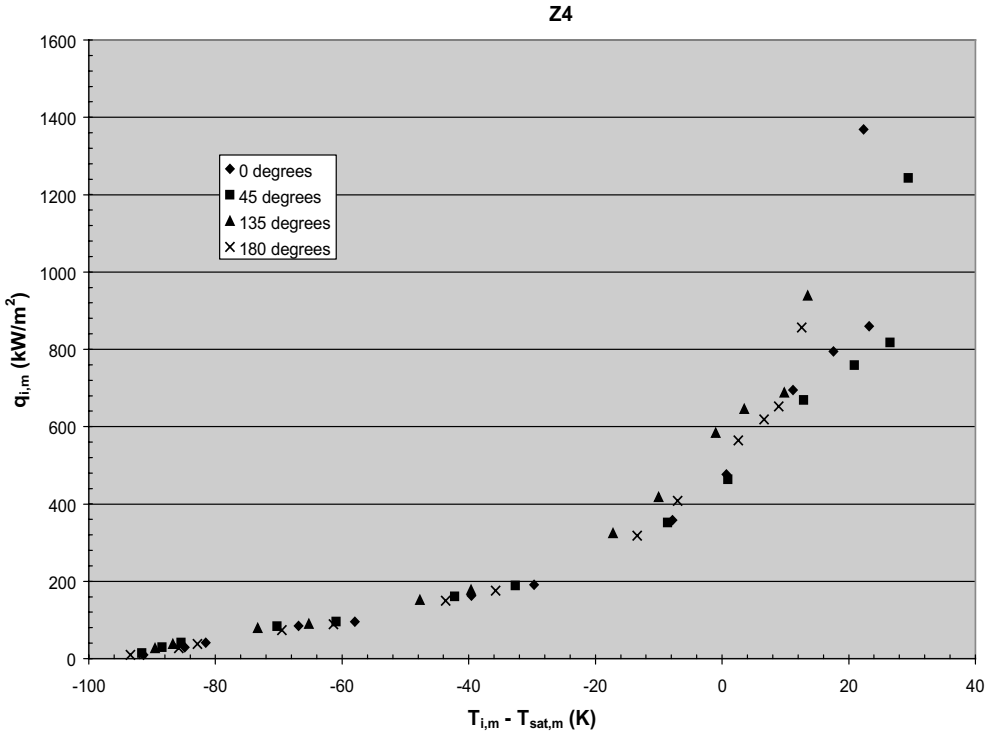

Fig. 11. Local (2-D) water boiling curves at $z = z4 = 192.09$ mm as a function of the circumferential coordinate with $\phi = 0°$ and 180° corresponding to the heated and cooled portions, respectively, of the plane of symmetry of the test section.

8. Conclusions

Conjugate heat transfer measurements involving water-subcooled flow boiling inside a single-side heated circular cylinder has resulted in three-dimensional local channel wall temperature measurements for a Reynolds number of 6900 and inside wall heat fluxes up to 1.35 MW/m^2. This data was used to generate two-dimensional inside flow channel wall: (1) boiling curves, (2) heat flux distributions, and (3) wall temperature distributions. All the HHFR data were tabulated for thirteen power levels ranging from single-phase flow up to fully-developed subcooled flow boiling. These single-side heated circular flow channel data are among the first set of conjugate data displaying local three-dimensional wall temperature and two-dimensional inside heat flux and wall temperature variations.

Acknowledgements

The authors are appreciative to the United States Department of Energy and Dr. Michael Crisp for their support of this work under contract #DEFG03-97ER54452. In addition, the authors and the TSRC Personnel acknowledge Mrs. Vivian Pope's support in every aspect of this work. Finally, a note of thanks goes to Avione Northcutt for geometrically characterizing the test section.

References

[1] R. Tivey, T. Ando, A. Antipenkov, V. Barabash, S. Chiocchio, G. Federici, C. Ibbott, R. Jakeman, G. Janeschitz, R. Raffray, M. Akiba, I. Mazul, H. Pacher, M. Ulrickson, G. Vieider, ITER divertor, design issues and research and development, Fusion Engineering and Design 46 (1999) 207–220.

[2] R. Tivey, M. Akiba, D. Driemeyer, I. Mazul, M. Merola, M. Ulrickson, ITER R&D: vacuum vessel and in-vessel components: divertor cassette, Fusion Engineering and Design 55 (2001) 219–229.

[3] A.R. Raffray, J. Schlosser, M. Akiba, M. Araki, S. Chiocchio, D. Driemeyer, F. Escourbiac, S. Grigoriev, M. Merola, R. Tivey, G. Vieider, D. Youchison, Critical heat flux analysis and R&D for the design of the ITER divertor, Fusion Engineering and Design 45 (1999) 377–407.

[4] M. Merola, G. Vieider, M. Bet, I. BobinVastra, L. Briottet, P. Chappuis, K. Cheyne, G. Dell'Orco, D. Duglué, R. Duwe, S. Erskine, F. Escourbiac, M. Fèbvre, M. Grattarola, F. Moreschi, A. Orsini, R. Pamato, L. Petrizzi, L. Plöchl, B. Riccardi, E. Rigal, M. Rödig, J.F. Salavy, B. Schedler, J. Schlosser, S. Tähtinen, R. Vesprini, E. Visca, C.H. Wu, European achievements for ITER high heat flux components, Fusion Engineering and Design 56–57 (2001) 173–178.

[5] G. Vieider, M. Merola, J.P. Bonal, P. Chappuis, D. Duglué, R. Duwe, F. Escourbiac, M. Fèbvre, L. Ginacarli, M. Grattarola, G. LeMarois, H.D. Pacher, A. Pizzuto, L. Plöchl, B. Riccardi, M. Rödig, J. Schlosser, I. Smid, P. Tramier, C.H. Wu, European development of the ITER divertor target, Fusion Engineering and Design 46 (1999) 221–228.

[6] G. Vieider, M. Merola, F. Anselmi, J.P. Bonal, P. Chappuis, G. Dell'Orco, D. Duglué, R. Duwe, S. Erskine, F. Escourbiac, M. Fèbvre, L. Giancarli, M. Grattarola, G. LeMarois, H.D. Pacher, A. Pizzuto, L. Plöchl, B. Riccardi, M. Rödig, J. Schlosser, A. Salito, B. Schedler, C.H. Wu, European development of prototypes for ITER high heat flux components, Fusion Engineering and Design 49–50 (2000) 135–143.

[7] T. Hino, M. Akiba, Japanese developments of fusion reactor plasma facing components, Fusion Engineering and Design 49–50 (2000) 97–105.

[8] M. Akiba, S. Suzuki, Overview of the Japanese mock-up tests for ITER high heat flux components, Fusion Engineering and Design 39–40 (1998) 219–225.

[9] R.E. Nygren, Actively cooled plasma facing components for long pulse high power operation, Fusion Engineering and Design 60 (2002) 547–564.

[10] C.B. Baxi, C.P.C. Wong, Review of helium cooling for fusion reactor applications, Fusion Engineering and Design 51–52 (2000) 319–324.

[11] M. Merola, L. Plöchl, Ph. Chappuis, F. Escourbiac, M. Grattarola, I. Smid, R. Tivey, G. Vieider, Manufacturing and testing of a prototypical divertor vertical target for ITER, Journal of Nuclear Materials 283–287 (2000) 1068–1072.

[12] G.W. Wille, K.T. Slattery, D.E. Driemeyer, G.D. Morgan, Development of 316L(n)-IG stainless steel fabrication approaches for ITER divertor and limiter applications, Fusion Engineering and Design 39–40 (1998) 499–504.

[13] T. Hatano, S. Suzuki, K. Yokoyama, T. Suzuki, I. Tokami, K. Kitamura, T. Kuroda, M. Akiba, H. Takatsu, High heat flux testing of a hip bonded first wall panel with built-in circular cooling tubes, Fusion Engineering and Design 39–40 (1998) 363–370.

[14] M.A. Ulrickson, J.N. Brooks, D.E. Driemeyer, A. Hassenein, C.E. Kessel, T. Rognlien, J.C. Wesley, D.M. Meade, Physics basis for the fusion ignition research experiment plasma facing components, Fusion Engineering and Design 58–59 (2001) 907–912.

[15] C.B. Baxi, Thermal hydraulics of water cooled divertors, Fusion Engineering and Design 56–57 (2001) 195–198.

[16] R.E. Nygren, High quality actively cooled plasma-facing components for fusion, Fusion Engineering and Design 28 (1995) 3–12.

[17] P.H. Chappuis, F. Escourbiac, M. Lipa, R. Mitteau, J. Schlosser, Possible divertor solutions for a fusion reactor. Part 2. Technical aspects of a possible divertor, Fusion Engineering and Design 36 (1997) 109–117.

[18] M. Rödig, M. Akiba, P. Chappuis, R. Duwe, M. Fèbvre, A. Gervash, J. Linke, N. Litounovsky, S. Suzuki, B. Wiechers, D.L. Youchison, Comparison of electron beam test facilities for testing of high heat flux components, Fusion Engineering and Design 51–52 (2000) 715–722.

[19] J. Boscary, M. Araki, J. Schlosser, M. Akiba, F. Escourbiac, Dimensional analysis of critical heat flux in subcooled water flow under one-side heating conditions for fusion application, Fusion Engineering and Design 43 (1998) 147–171.
[20] J. Boscary, J. Fabre, J. Schlosser, Critical heat flux of water subcooled flow in one-side heated swirl tubes, International Journal of Heat and Mass Transfer 42 (2) (1999) 287–301.
[21] F. Inasaka, H. Nariai, Enhancement of subcooled flow boiling critical heat flux for water in tubes with internal twisted tapes under one-sided-heating conditions, Fusion Engineering and Design 39–40 (1998) 347–354.
[22] G.P. Celata, M. Cumo, Y. Katto, A. Mariani, Prediction of the critical heat flux in water subcooled flow boiling using a new mechanistic approach, International Journal of Heat and Mass Transfer 42 (8) (1999) 1457–1466.
[23] G.P. Celata, M. Cumo, A. Mariani, G. Zummo, The prediction of the critical heat flux in water-subcooled flow boiling, International Journal of Heat and Mass Transfer 38 (6) (1995) 1111–1119.
[24] W. Liu, H. Nariai, F. Inasaka, Prediction of critical heat flux for subcooled flow boiling, International Journal of Heat and Mass Transfer 43 (18) (2000) 3371–3390.
[25] G.P. Celata, M. Cumo, A. Mariani, G. Zummo, Physical insight in the burnout region of water-subcooled flow boiling, Revue Générale de Thermique 37 (6) (1998) 450–458.
[26] G.P. Celata, M. Cumo, A. Mariani, G. Zummo, Burnout in subcooled flow boiling of water. A visual experimental study, International Journal of Thermal Sciences 39 (9–11) (2000) 896–908.
[27] R.D. Boyd, Similarities and differences between single-side and uniform heating for fusion applications-I: uniform heat flux, Fusion Technology 25 (1994) 411–418.
[28] R.D. Boyd, P. Cofie, Q.-Y. Li, A.A. Ekhlassi, A new facility for measurements of three-dimensional, local subcooled flow boiling heat flux and related critical heat flux for PFCs, Fusion Science and Technology 41 (2002) 1–12.
[29] R.D. Boyd, P. Cofie, A.A. Ekhlassi, M. Strahan, Conjugate heat transfer measurements in a single-side heated circular flow channel under turbulent, subcooled flow boiling conditions, Twelfth International Heat Transfer Conference, Elsevier SAS, Grenoble, France, 2002, pp. 713–718.